Environmental Science & Technology

pubs.acs.org/est

Article

Enhanced Bacterium–Phage Symbiosis in Attached Microbial Aggregates on a Membrane Surface Facing Elevated Hydraulic Stress

Yixiao Tan, Pingfeng Yu,* Dan Huang, Mengting Maggie Yuan, Zhuodong Yu, Huijie Lu, Pedro J.J. Alvarez, and Liang Zhu*

Cite This: *Environ. Sci. Technol.* 2023, 57, 17324–17337

Read Online

ACCESS | Metrics & More | Article Recommendations | Supporting Information

ABSTRACT: Phages are increasingly recognized for their importance in microbial aggregates, including their influence on microbial ecosystem services and biotechnology applications. However, the adaptive strategies and ecological functions of phages in different aggregates remain largely unexplored. Herein, we used membrane bioreactors to investigate bacterium–phage interactions and related microbial functions within suspended and attached microbial aggregates (SMA vs AMA). SMA and AMA represent distinct microbial habitats where bacterial communities display distinct patterns in terms of dominant species, keystone species, and bacterial networks. However, bacteria and phages in both aggregates exhibited high lysogenicity, with 60% lysogenic phages in the virome and 70% lysogenic metagenome-assembled genomes of bacteria. Moreover, substantial phages exhibited broad host ranges (34% in SMA and 42% in AMA) and closely interacted with habitat generalist species (43% in SMA and 49% in AMA) as adaptive strategies in stressful operation environments. Following a mutualistic pattern, phage-carried auxiliary metabolic genes (pAMGs; 238 types in total) presumably contributed to the bacterial survival and aggregate stability. The SMA-pAMGs were mainly associated with energy metabolism, while the AMA-pAMGs were mainly associated with antioxidant biosynthesis and the synthesis of extracellular polymeric substances, representing habitat-dependent patterns. Overall, this study advanced our understanding of phage adaptive strategies in microbial aggregate habitats and emphasized the importance of bacterium–phage symbiosis in the stability of microbial aggregates.

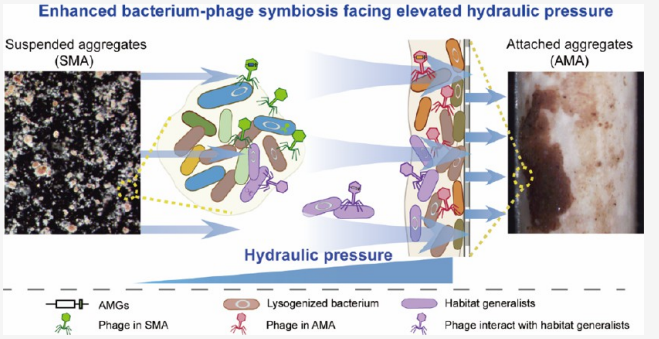

KEYWORDS: *microbial aggregates, bacterium–phage interactions, habitat generalists, adaptive strategy, auxiliary metabolic genes*

INTRODUCTION

Microbial aggregates are surface- or self-attached microbial consortia encased in a mucilaginous matrix of extracellular polymeric substances (EPSs).[1] Due to their enhanced metabolism and environmental tolerance,[2] microbial aggregates are the dominant forms of microbes in natural[3] and biotechnological systems.[4] Microbial aggregates thus received growing interest for their ecological implications[5] and technological contributions (e.g., resource conservation and contaminant degradation).[6] Notably, the stability and function of microbial aggregates are closely associated with microbial interactions within aggregates.[7,8] Additionally, the surface- and self-attached forms represent distinct habitats, which are reported to be induced by hydraulic pressure.[9] Due to the distinct aggregate scale and structural heterogeneity, the surface-attached habitats may exhibit different microbial interactions due to the facilitated metabolism and high resistance to environmental stressors.[10,11] Therefore, it is critical to elucidate the microbial interactions within microbial aggregates to harness their full ecological and biotechnological potential.

Phages are bacterial viruses that are increasingly recognized for their prevalence and importance in microbial communities.[12] Phages can mediate bacterial mortality and metabolism through lytic and lysogenic infections, which further influence the microbiome structure and functions.[13,14] Especially, the biological reactors of wastewater treatment plants harbor highly abundant and diverse phages[15] that closely interact with their bacterial hosts.[16,17] Moreover, phages are potentially involved in mediating host metabolism by carrying extensive auxiliary metabolic genes (AMGs) associated with microbial

Received: July 11, 2023
Revised: October 12, 2023
Accepted: October 13, 2023
Published: November 6, 2023

carbon and nutrient cycling in this engineered system.[18,19] Recent researchers have uncovered the variation of bacterium−phage interactions in response to environmental stress.[20,21] However, it remains largely unexplored how microbial aggregate habitats (and their associated microenvironments) influence bacterium−phage interactions and virome functions. Therefore, it is crucial to illuminate bacterium−phage interactions in microbial aggregates of engineered systems.

Membrane bioreactors (MBRs) are a promising technology applied widely in wastewater treatment systems.[22] Specifically, MBRs contain suspended loose microbial aggregates (i.e., activated sludge flocs responsible for pollutant degradation), while tightly attached microbial aggregates (i.e., attached foulant layer responsible for membrane fouling) are formed on the membrane surface. Thus, MBRs are a model engineered system for studying bacterium−phage interactions in different aggregates. Meanwhile, the robustness of MBR systems to influent fluctuation, stable microbial profile in activated sludge flocs, and regular formation of membrane foulant under artificial upholding facilitate the comparison of microbial interactions due to habitat differences.[23,24] Elucidating bacterium−phage interactions in MBRs could not only advance our understanding of microbial interactions in microbial aggregates but also inspire ecological strategies for performance enhancement in engineered systems.[25]

This study investigated the phage composition and bacterium−phage interactions in suspended and attached microbial aggregates. The aggregates from a full-scale MBR were analyzed in terms of the surface morphology and EPS profile. Metagenomic analysis was conducted to reveal the generalist and keystone species in the representative microbial aggregates. Viromic analysis was adopted to illuminate phage composition, lysogenicity, and bacterium−phage interactions. The phage-carried AMGs were systematically analyzed to reveal the potential contributions of phages to the microbial structural and functional stability. These findings provide crucial insights into bacterium−phage interactions in microbial aggregates and reveal the potential of phages for the stability and function of microbial aggregates.

MATERIALS AND METHODS

Full-Scale MBR Operation and Microbial Aggregate Sampling. The full-scale buried MBR was located in Hangzhou, China (30°15′00.00″ N,120°10′00.00″ E), and the membrane modules were immersed in the aerobic area. The floc activated sludge (labeled as the SMA group for suspended microbial aggregates) and membrane foulant (labeled as the AMA group for attached microbial aggregates) were sampled three times as biological replicates in winter and summer, respectively. Specifically, the attached membrane foulant was scraped off the membrane fibers of the suspended MBR modules. The floc activated sludge was collected in the MBR tanks after plain sedimentation during the same operation period. The water qualities of influent and effluent in the MBR unit during the sampling period were both characterized in terms of total phosphorus (TP), NH_3, total nitrogen (TN), chemical oxygen demand (COD), biochemical oxygen demand (BOD_5), and suspended solid (SS) according to the standard procedures,[26] as well as the microbial aggregate properties in terms of TN and total organic carbon (TOC). The influent and effluent parameters and hydraulic pressure are shown in Figures S1 and S2 in the Supporting Information.

Analysis of Microbial Aggregate Structures. Stereo microscopes (LEICA M50, Germany) were used to visualize microbial aggregates. Scanning electron microscopy (SEM) (FEI QUANTA FEG 650, USA) was employed to characterize the surface morphology of sampled aggregates. Polysaccharide (PS) and protein (PN) in EPS were extracted using a heat extraction method as previously described.[27] The total PS and PN contents in EPS were then quantified by a UV−vis spectrophotometer (SHIMADZU UV-2600, Japan) using a phenol-sulfuric acid method and modified Lowry colorimetric method,[28,29] respectively. The EPS profile analysis conducted by a three-dimensional fluorescence excitation−emission matrix (EEM) was described in the Supporting Information Method S1. Four fluorescence components, mainly the humic-like substance and protein-like substance (i.e., humic-like compounds derived from microbial activities (C1), humic-like compounds with higher aromaticity (C2), tyrosine-like or tryptophan-like protein substances (C3), and fulvic acids (C4)), were separated by the PARAFAC analysis of EEM spectra data.

Microbial DNA Extraction, Metagenome Sequencing, and Assembly. The total microbial DNA was extracted from sludge samples using Qiagen DNeasy PowerSoil Kits following the manufacturer's instructions. Qualified DNA samples were determined by NanoDrop Microvolume Spectrophotometers (ThermoFisher Scientific, US). Sequencing libraries were generated using an NEB Next Ultra DNA Library Prep Kit for Illumina (New England Biolabs, MA, USA) following manufacturer's recommendations. The library was sequenced on an Illumina NovaSeq 6000 platform (Illumina Inc., USA) to obtain 150 bp paired-end reads (PE150 mode). The quality control of raw reads was conducted by Trimmomatic (v0.26)[30] followed by high-quality reads assembled by MEGAHIT (v1.1.2)[31] with default parameters. Thereafter, CD-HIT (v4.7)[32] was used to remove redundancy and obtain unigenes (i.e., the nucleotide sequences coded by unique and continuous genes), which is clustered by identity 95%, coverage 90%, and the longest sequences of which were chosen as representative sequences. MetaGeneMark-2[33] was used to predict the open reading frame (ORF), and BBMAP v38.96[34] was adopted to calculate the abundance of contigs and genes.

Bacterial Taxonomic Assignment, Functional Annotation, and Generation of Metagenome-Assembled Genomes. Taxonomy prediction of the bacterial contigs was conducted by Diamond by matching the unigenes against the NCBI NR database with an *e*-value of 1×10^{-5}. Functional genes were annotated using Diamond with an *e*-value of 1×10^{-5} by matching to the KEGG database (Released 101.0). The assembled contigs of each sample were binned by the binning module within metaWRAP (v1.2.2)[35] with parameter "--metabat2 --maxbin2 --concoct --run-checkm" followed by the bin-refinement module with parameters "-c 70 -x 10". A total of 176 high-quality bins with completeness >70% and contamination <10% were identified as bacterial metagenome-assembled genomes (MAGs), the relative abundance of which was calculated by using quant-bins module within metaWRAP (v1.2.2) with default parameters. Taxonomic annotation of MAGs was conducted by GTDB-Tk (v2.1.1)[36] based on the database Genome Taxonomy Database (http://gtdb.ecogenomic.org, Release207). To minimize the loss of information about bacterial communities, the bacterial

https://doi.org/10.1021/acs.est.3c05452
Environ. Sci. Technol. 2023, 57, 17324−17337

scaffolds were used in the subsequent analysis due to the limitations of MAGs in the associated approaches.

Identification of Habitat Specific Species, Keystone Species, and Habitat Generalist Species. The habitat-associated features of the microbial community are depicted by the abundance, occurrence, and connectivity of species. Briefly, the habitat specific species of each sample group were first estimated by LEfSe analysis with an LDA cutoff of 2.0[37] to screen out the specific species in each sample group and then clustered by the hierarchical clustering method. Twelve taxa with relative abundance >0.1% and mainly distributed in the AMA or SMA group were chosen as the biomarkers. Keystone species of each habitat were identified by a network analysis workflow (Method S2) and visualized by Gephi (v 0.9.2).[38,39] Then, keystone species were determined by within-module connectivity (Zi) and among-module connectivity (Pi) values with module hubs (Zi > 2.5) and connectors (Pi > 0.62) regarded as keystone species.

Habitat generalists are reported to contribute to the environmental adaptivity of microbial communities.[40] The species were identified as habitat generalists if the following criteria were satisfied simultaneously: niche breadth value >95%, dissimilarity score >10%, and relative abundance >1 × 10^{-4}.[41] The niche breadth scores of species (n = 12) were estimated by "Levins" and "Shannon" methods using the "spaa" package in R (https://github.com/helixcn/spaa). The dissimilarity scores were calculated based on the mean of pairwise dissimilarity across habitats as below:[42]

$$\text{dissimilarity scores} = \frac{\sum_i^n \sum_j^n c_i c_j,\ i \neq j}{n^2 - n}$$

with $c_i c_j$ being the Spearman's rank correlation coefficient (c, $0.5 - (\rho/2)$) of species in each habitat. A species with a high dissimilarity score means to it is present in samples with dissimilar microbial profiles. The identified habitat generalists across microbial aggregates are summarized in Table S2.

Phage Particle Collection, Characterization, and Phage DNA Extraction. Phage particles in the raw samples were concentrated through filtration and ultrafiltration centrifugation following the reported protocol.[43] Briefly, the sludge was pretreated with potassium citrate buffer and then sonicated to release the phage particles. The suspension was centrifuged to remove larger impurities, and then, the supernatant was filtered sequentially through 0.45 and 0.22 μm filters to obtain the filtrate containing phages. The phages were then enriched by tangential flow filtration (TFF, Sartorius Vivaflow50 30,000 MWCO PES, USA) followed with ultrafiltration centrifugation (Sartorius Vivaspin 30,000 MWCO PES, USA). The phage concentrate was verified by electron microscopy imaging using a transmission electron microscope (TEM, JEOL 1010, Japan). Fluorescence microscopy imaging (LEICA DM2000, Germany) was employed to assess the viral-like particles (VLPs) stained by SYBR GOLD as in a previous study.[44] The measurement of the virus-to-bacteria ratio is described in Method S3. For viral DNA extraction, the phage concentrate was treated with DNase I (Thermo Scientific) to remove nonencapsulated DNA fragments and then subjected to phage DNA extraction by a Qiagen AllPrep PowerViral DNA/RNA Kit.

Phage Sequence Identification and Taxonomic Classification. The extracted phage DNA was whole-genome amplified using a KAPA HiFi HotStart ReadyMix. The library was sequenced on an Illumina NovaSeq 6000 platform, and clean data was obtained by Trimmomatic (v0.36) with default parameters. The MEGAHIT (v1.1.2, parameter: --presets meta-large --min-contig-len 300) and CDHIT (v4.7, parameter: -c 0.95 -aS 0.8) were used to control sequence quality and obtain unique contigs. Then, the viral sequences were screened through the customized process "Virsorter2 (v2.1.0)[45] -CheckV (v0.7.0)[46] -Virsorter2" by default parameters of each tool and contig length >5kb as previously described.[43] This pipeline coupling Virsorter2 and CheckV could guarantee the quality of obtained phage contigs by checking completeness and contamination and minimizing the loss of phage diversity. The output viral sequences of CheckV (v0.7.0) in the second step with "high-quality" were considered. Virsorter2 (v2.1.0) in the third step was used to identify the outcome phage contigs by default parameters with "max_score" > 0.7 along with DeepVirFinder (v1.0)[47] with q-value <0.01 as the cutoff. Phage contigs were determined by using BWA-MEM to map individual reads to the contigs, and the relative abundance of which was calculated as reads per kilobase per million mapped reads (RPKM) by SAMtools (v1.9).[48] All identified viral genomes were taxonomically classified and clustered with viral genomes from the NCBI Viral RefSeq database by vConTACT2 (v0.9.19).[49] The lifestyle of phage contigs was identified by DeePhage (v1.0)[50] (virtual machine version), PhaTYP[51] (https://phage.ee.cityu.edu.hk/), and lysogenic markers detection by using hmmscan based on the list of lysogenic markers genes (transposase, integrase, excisionase, resolvase, and recombinase) from Pfam-A database[52] (Table S9). DeePhage (v1.0) was used to identify phage lifestyle with 0.5 as the cutoff of lysogeny, which was verified by the above PhaTYP online version. In addition, CheckV and DeepVirFinder were used to identify the prophage contigs (≥1 kbp) from prokaryotic scaffolds by default parameters and q-value <0.01 as the cutoff. The relative abundance of prophage contigs was also calculated based on the relative abundance of the prokaryotic scaffolds and expressed as RPKM. Further, to obtain phage contigs of high quality and lower the complexity of phage communities, phage contigs were clustered into viral operational taxonomic units (vOTUs) using the CheckV package[46,53] based on pairwise average nucleotide identity (ANI) with recommended parameters (95% ANI + 85% AF (AF, alignment fraction)) (Table S4). vConTACT2 (v0.9.19)[49] was employed to explore the overlap of vOTUs with phage sequences from the human gut virome database (GVD),[54,55] global ocean database (GOV),[56] IMG/VR 4.0 database (IMGVR v4.0),[57] and NCBI Refseq database (Refseq) by affiliating VCs with shared proteins. To ensure reliability of the results, subsequent downstream analyses were also performed for high-quality vOTUs (CheckV completeness >70%) in parallel.

Phage Host Prediction and Bacterium−Phage Interaction Analysis. The obtained vOTUs were linked with their putative hosts with prognostic computational approaches based on the bacterial scaffolds (considering that short reads of tRNA and spacer may not be assembled into the MAGs), including clustered Regularly Interspaced Short Palindromic Repeats (CRISPR) spacer, tRNA, and prophage genome homology (Table S5). CRISPR spacers were separately recovered from bacterial sequences and vOTUs using CRISPRCasFinder[58] with default parameters. Then, the CRISPR spacers in the bacterial genome were searched against all viral elements with a query coverage of ≥90% and an e-value ≤10^{-4}

https://doi.org/10.1021/acs.est.3c05452
Environ. Sci. Technol. 2023, 57, 17324−17337

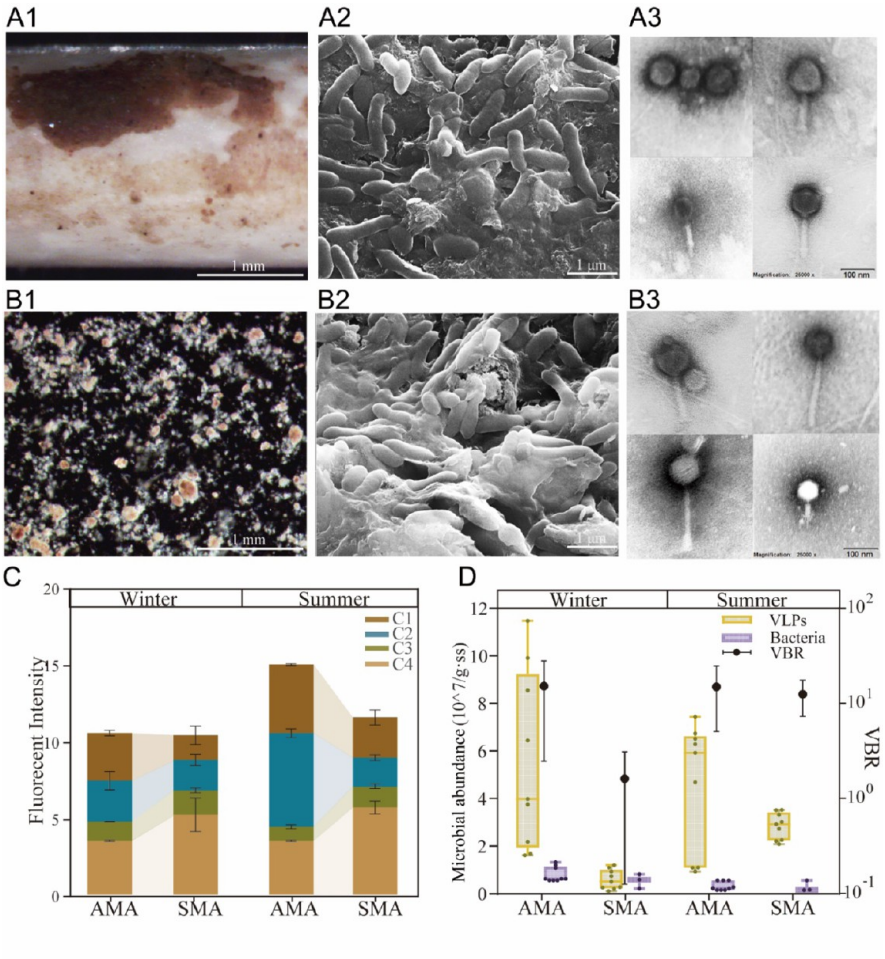

Figure 1. Structure and composition of suspended and attached aggregates. Attached microbial aggregates on the membrane module were characterized with (A1) stereo microscope imaging, (A2) SEM imaging, and (A3) phage particle analysis using TEM. Suspended microbial aggregates were characterized with (B1) stereo microscope imaging, (B2) SEM imaging, and (B3) phage particle analysis using TEM. (C) EPS profile of the suspended and attached aggregates in summer and winter. C1 represents humic-like compounds derived from microbial activities, C2 represents humic-like compounds with higher aromaticity, C3 represents tyrosine-like or tryptophan-like protein substances, and C4 represents fulvic acids. AMA and SMA refer to attached and suspended microbial aggregates, respectively. (D) Abundance of bacteria and phages in microbial aggregates reflected by 16S rRNA gene copy numbers (purple bars) and the fluorescence microscopic counting of VLPs (yellow bars), respectively. The virus−bacterium ratio (VBR) was calculated as phage abundance versus bacterial abundance in each sample. Error bars represent the standard deviation from at least triplicates.

to obtain the best hit. All the tRNA genes from vOTUs and bacterial sequences were identified by tRNAscan-SE (v2.0.9)[59] using the general and bacterial models, respectively. The tRNA genes identified in vOTUs were aligned against the local blastdb of tRNA genes of bacterial scaffolds using BLASTn with an *e*-value of 1×10^{-10}. For prophage genome homology match, the microbial genomes aligned with vOTUs using BLASTn with the *e*-value 1×10^{-10}, 95% nucleotide similarity, and matching length ≥1 kbp. The hosts of all viral contigs were also predicted based on public databases IMG/VR 4.0[57] with *e*-value 1×10^{-10}. These results were verified by CHERRY[60] with accuracy >90% and score = 1.

Identification and Analysis of Phage-Carried Auxiliary Metabolic Genes. The potential auxiliary metabolic genes in phage contigs were predicted by DRAM-v in DRAM[61] and VIBRANT (v1.2.0).[62] The pAMGs were identified by DRAM-v with auxiliary scores >3 and flagged with "M" were chosen.[63] The AMG identification by VIBRANT was conducted with default parameters in "virome" mode and 4 ORFs per scaffold to limit input sequences.[62] All pAMGs were annotated based on Kofam, PFAM, NCBI Viral RefSeq, and VOGDB database. In addition, the pAMGs carried by high-quality vOTUs (654 in total) were excavated and analyzed in parallel (Table S6). The reported pAMGs were encoded in the phage contigs with lengths >10 kbp and putative prophage contigs with lengths >5 kbp. Due to the limitations in the identification of prophage-carried AMGs, the reported prophage contigs were also assessed by Deepvirfinder with *q*-value <0.05 or CheckV completeness method marked with AAI-based high-confidence and medium-confidence (Table S7). The metabolic pathways involved in pAMGs were annotated based on the KEGG database. The lysogenic marker proteins identified in phage contigs were verified based on the Pfam database.[52] Promoters and terminators of contigs were predicted by BPROM and FindTerm on the platform Softberry (www.softberry.com) with default parameters, respectively.[44] Bakta[64] was used to annotate the reference genes of reported pAMGs from the local prokaryotic sequences with default parameters (light version database). The phylogenetic trees of the reported pAMGs with reference

https://doi.org/10.1021/acs.est.3c05452
Environ. Sci. Technol. 2023, 57, 17324−17337

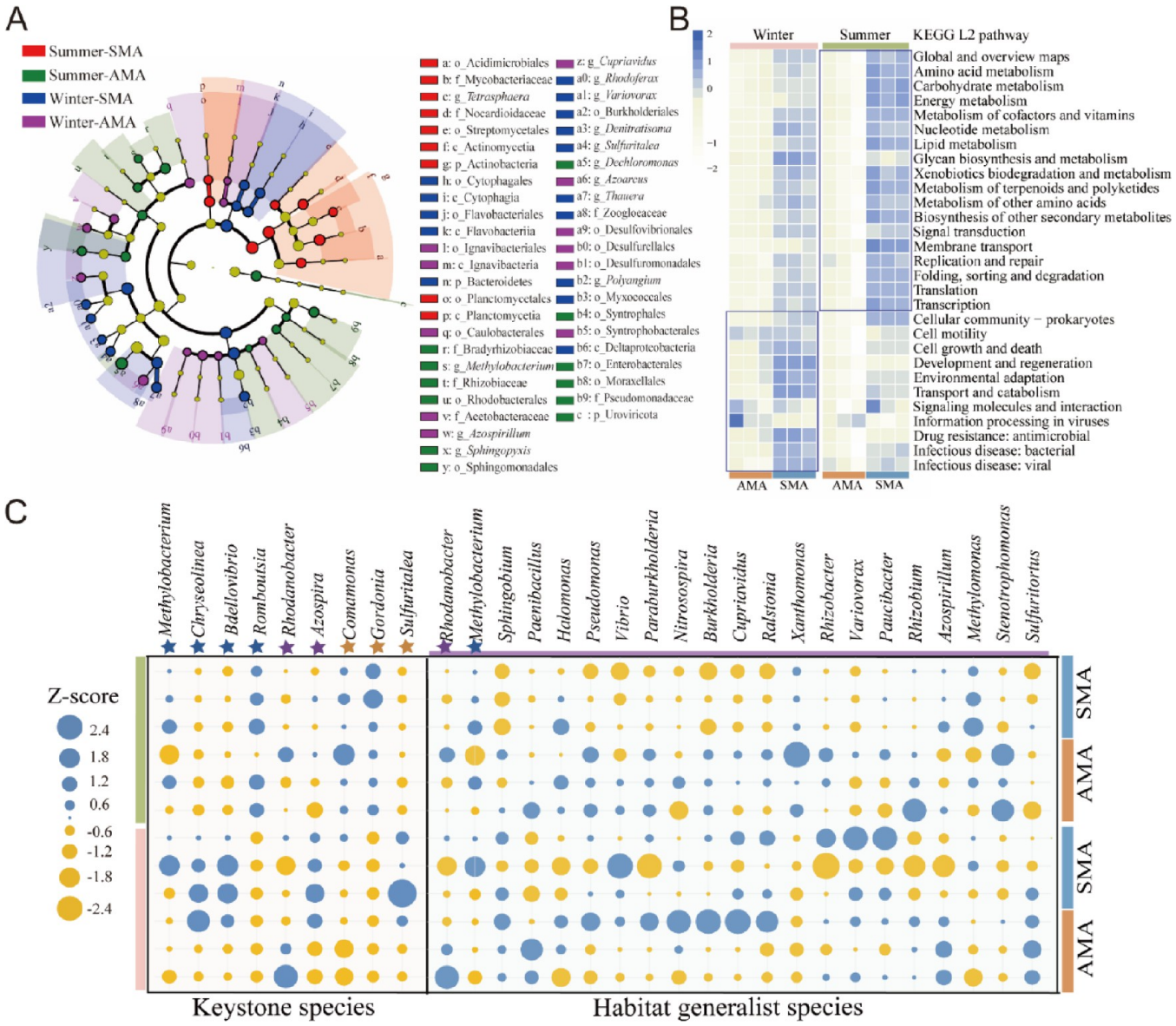

Figure 2. Dynamics of the microbial composition of microbial aggregates. (A) Cladogram of the phylogenetic distribution of microbial lineages of LEfSe analysis (n = 3) associated with four sample groups. Differences in all ranks are represented by the color (red indicating the summer SMA group, green for summer AMA, blue for winter SMA, and purple for winter AMA). (B) Heatmap profiles of microbial communities' functional categories (KEGG level 2). The upper part of pathways is related to cell metabolisms, and the lower part is related to cell lifecycles. (C) Heatmap analysis of the species of interest identified in this study. The Z-score represents the enrichment level of species in each sample group, and its value is reflected by circle color and size (blue for positive values and yellow for negative, with circle size representing the absolute value). Specifically, nine keystone species were identified by network analysis, and those of SMA only, AMA only, and shared by both groups were marked with asterisks in blue, orange, and purple, respectively. Twenty-one species exhibiting broad niche width and abundance in both types of aggregates were identified as habitat generalist species (marked with the purple dash).

genes from the NCBI database and local prokaryotic sequences were constructed based on the maximum likelihood method by MEGA11.[65] To further support the possible function of pAMGs in virome, the predicted tertiary protein structures of which were constructed online by phyre2 (v2.0) with 100% confidence score and alignment coverage above 70%.[66] SWISS-Model was then used to predict the quaternary structure of each protein with a Global Model Quality Estimation (GMQE) score above 0.6[67] (Table S8). Moreover, the predicted structures were compared to the public protein databases Uniprot[68] and RCSB PDB database.[69] The detailed process is described in Method S4.

Statistical Analysis. Statistical analysis was conducted and visualized by the R (version 4.2.3) platform and GraphPad Prism9. The microbial alpha- and beta-diversity analysis, redundancy analysis (RDA), principal component analysis (PCA), and Mantel's test were performed using the package "dplyr", "ggcor", "vegan", and "ggplot2" in R. Linear discriminant analysis effect size (LEfSe) analysis of microbial composition was performed on the Galaxy platform (https://huttenhower.sph.harvard.edu/galaxy/). The overall mean differences of samples were analyzed using the One Sample t test by GraphPad Prism9. Other statistical analyses were conducted and visualized with Cytoscape (v3.7.2) and Chiplot (https://www.chiplot.online/).

https://doi.org/10.1021/acs.est.3c05452
Environ. Sci. Technol. 2023, 57, 17324−17337

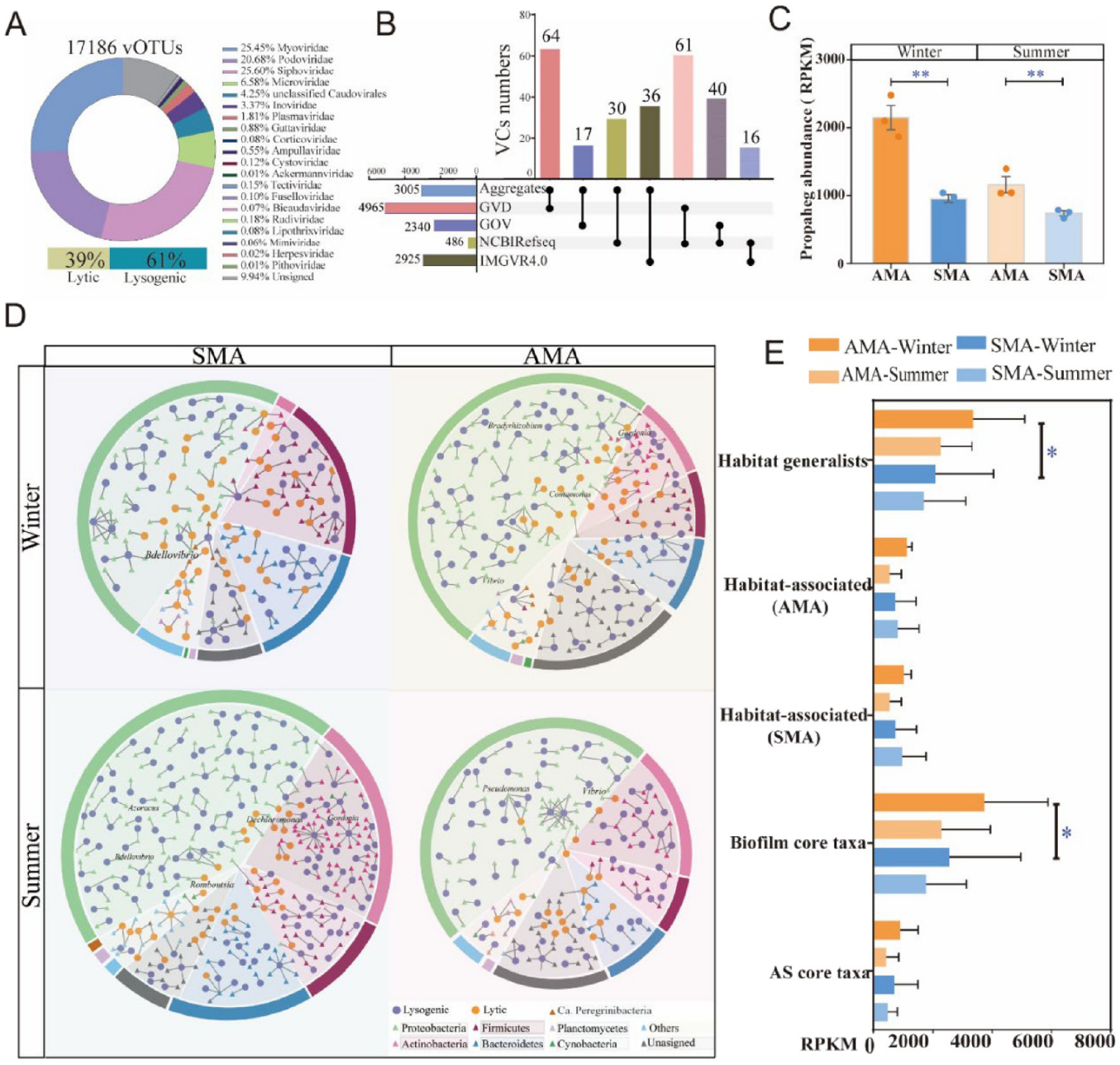

Figure 3. Dynamics of phage communities and bacterium−phage interaction in different habitats. (A) Composition and lysogeny ratio of vOTUs based on the merged virome of the MBR unit. (B) Shared VC numbers of microbial aggregate virome with the reference viral sequences from public databases GVT, GOV, IMGVR4.0, and NCBI RefSeq (ProkaryoticViralRefSeq94 database in vContact2). (C) Abundance of prophage contigs in each group (t test, ** $p < 0.01$). (D) The dynamics of phage−host linkages in aggregates (predicted by prognostic computational methods) are displayed by the network diagram of vOTUs−phage pairs in each sample group. The nodes representing the vOTUs of the lytic and lysogenic lifestyle were in yellow and purple, respectively. The doughnut chart outside the networks diagram shows the distribution of hosts in different phyla. (E) Relative abundance of phage contigs linked to bacterial clusters using public databases. The host species detected in less than two samples were eliminated. All the dots and error bars of the SMA and AMA groups were in blue and orange, respectively (t test, * $p < 0.05$).

RESULTS AND DISCUSSION

Suspended and Attached Aggregates Represented Distinct Microbial Habitats. The suspended aggregates (SMA) and attached aggregates (AMA) exhibited different morphologies and EPS components under distinct hydraulic pressures (0.5 kPa vs 20.7 kPa) and wastewater treatment operation (e.g., AMA exposed to aeration bubbles and membrane cleaning chemicals). The AMA formed a compact biofilm on the membrane surface, while SMA displayed irregular forms of flocs (Figure 1A,B), representing distinct microbial habitats. As a major contributor to the structural stability of aggregates, EPS components also differed by habitat. Notably, AMA-summer harbored higher levels of EPS (3.5-fold) relative to SMA-summer, whereas a slight difference was seen in the winter group (Figure S4B). The high concentration of PS (2.1-fold) and high PS/PN ratio in AMA-summer potentially associated with the microbial response to the external stimulus,[70] while the discrepant PS/PN ratio in AMA-winter (standard deviation (SD): 0.35 vs 0.23) relative to SMA indicated unsteady cell aggregation. The

https://doi.org/10.1021/acs.est.3c05452
Environ. Sci. Technol. 2023, 57, 17324−17337

drastic hydraulic pressure on the membrane surface (20.7 kPa vs 0.5 kPa, relative to SMA; Figure S2) may pose a great threat to microbial aggregation. The excessive excretion of PS in AMA-summer, which increased the cross-linking within the aggregates,[71] potentially contributed to the rigidity of aggregates under hydraulic shear force.

In addition, the more adverse habitats in winter were in accordance with the lower biodiversity and evenness of microbial communities (Figure S5A,B). The microbiome in AMA carried lower abundances of functional genes associated with microbial metabolism (Figure S5C), consistent with the lower amount of microbial activity-derived substance relative to SMA (C3, 0.6-fold; Figure 1C). Moreover, the larger amount of humic in AMA (C2, 1.4-fold), which potentially contributed to the heterogeneous composition and toxicants adsorption, exhibited lower bioavailability in aggregate[72] and might be associated with the nutrient condition in the AMA. These results indicated that besides the seasonality, the high hydraulic pressure on the membrane surface, along with other environmental stresses, potentially shaped the more hostile habitat environment for the microbes in AMA.

As expected, both microbial aggregates sheltered abundant and diverse phage particles (Figure 1A3,B3), with an average virus-to-bacteria ratio (VBR) of around 10 across all the samples (Figure 1D). Notably, AMA harbored higher phage levels relative to SMA (means: 4.29×10^7 vs 0.58×10^7 VLPs $g{\cdot}ss^{-1}$, $p < 0.05$), while the phage levels were more stable in SMA compared to AMA (SD: 0.36 vs 3.71 VLPs $g{\cdot}ss^{-1}$, $p < 0.05$). The variation of phage abundance corroborated that suspended and attached aggregates represented distinct microbial habitats. Together, the specific structure of microbial aggregates was mainly formed under the elevated hydraulic pressure on the membrane surface, thus altering the microenvironments of the attached aggregates.

Microbial Communities in Suspended and Attached Aggregates Displayed Distinct Patterns. Due to the proximity of SMA and AMA in the same bioreactor, their microbial communities reflected a continuum that shared several dominant phyla and habitat generalists. The similar microbial compositions on the phylum level were described by 14 dominant phyla widely distributed in wastewater treatment plants, such as *Proteobacteria* (59−72% of total abundance), *Actinobacteria* (3.8−19.3%), *Bacteroidetes* (2.9−10.4%), *Chloroflexi* (2.4−5.1%), *Nitrospira* (2.5−5.7%), and *Planctomycetes* (1.9−3.4%) (Figure S6A), consistent with that of qualified MAGs (Figure S6B). However, the core taxa differed between habitats, with typical activated sludge taxa[73] enriched in SMA and those of biofilm[23,24] enriched in AMA (Figure S6C, Table S2). For example, SMA harbored a significantly higher abundance of *Rhodoferax* (0.013‰ vs 0.010‰, $p < 0.05$) relative to AMA, while AMA enriched *Pseudomonas* (0.030‰ vs 0.026‰, $p < 0.05$).

Environmental stresses (e.g., nutrient limitation and hydrodynamic flushing) could influence the aggregate structure and microbial community.[9,74] The habitat featured microbial communities were characterized by habitat specific species and keystone species.[75,76] The habitat specific species of AMA community were well-recognized for versatile metabolic functions (Figure 2A and Figure S6D), such as sulfur metabolism (i.e., o_Desulfrellales)[77] and recalcitrant organics biodegradation (i.e., g_*Sphingopyxis*).[78] On the contrary, most of the habitat specific species in the SMA group were associated with nitrogen metabolism (i.e., g_*Azoracus*),[79] corresponding to nutrient removal in the upstream treatment process. Nine keystone species were identified on the genus level (Figure S7) that also corroborated microbial habitat difference (Figure 2C) and corresponding metabolic preference. Two of the keystone species (g_*Rhodanobacter* and g_*Azospira*) were shared in both habitats, in which g_*Rhodanobacter* associated with denitrification[80] was also identified as a habitat generalist.

We identified 21 habitat generalists (Figure 2C). Three of the keystone species were also highly abundant (relative abundance >0.1%) in the microbial aggregates. The habitat generalists tend to have broad interspecies interactions and are resistant to adverse biotic and abiotic stresses.[42] The generalists were accordingly more abundant in the AMA than in SMA (1.4% vs 1.3%, $p < 0.05$). Notably, these bacteria were well recognized for biodegradation (i.e., g_*Cupriavidus*),[81] nitrogen metabolism (i.e., g_*Nitrosospira*),[82] and biofilm formation (i.e., g_*Vibrio*),[83] indicating their significant contribution to microbial adaptation on the membrane surface and the functioning of the MBR system.

Microbial Aggregates Harbored Novel and Diverse Phage Communities. The importance of phage communities was increasingly recognized in microbial structures and functions.[14,19] A total of 17,186 vOTUs were clustered from free phage contigs (>5kb) identified from six SMA and six AMA samples (Table S3) and mainly belonged to 20 viral genera (Figure 3A). Tailed phages were dominant members (71.7% of vOTUs), supported by TEM imaging of the phage particles (Figure 1A3,B3). The 3005 viral clusters (VCs) from the MBR shared 64, 17, and 36 VCs with human gut virome (GVD), global ocean virome (GOV), and IMGVR 4.0 database, respectively (Figure 3B and Figure S8). The relatively high overlap between the MBR and human gut virome possibly reflected viral dispersion from the human gut to municipal wastewater.[84] The gut virome was over represented, possibly due to its predominance in the public databases. Approximately 61% of vOTUs in the MBR were identified as lysogenic (Figure 3A), which was significantly higher than that in other aquatic environments (∼20%)[85] and human gut virome (∼50%).[54] Collectively, these results corroborate the novelty and diverse virome in the activated sludge.[86] Incorporating more samples and bioreactors would strengthen our findings and provide additional valuable information, which is highly desired in future research.

In accordance with the bacterial communities, the phage communities in different habitats consisted of similar taxonomic compositions (Figure S8A). Moreover, the bacterial and phage communities (Figures S5A and S8B) showed good consistency of biological replicates in the same season, while the summer group of phages showed an overlap between habitats. Phage−host linkages were constructed to reveal the phage−bacterium interactions in microbial aggregates (Figure 3D). Mainly, 491 vOTUs were linked to 469 prokaryotic sequences after deduplication, with 5 by spacer matching, 70 by tRNA matching, and 416 by genome homology matching (Figure S9). The bacterial hosts were mainly distributed in phyla *Proteobacteria* (47%), *Actinobacteria* (12%), *Firmicutes* (13%), and *Bacteroidetes* (10%), which were the dominant phyla in the bacteria community (83%). Notably, about 70% of the qualified MAGs carried lysogenic markers (Figure S10A). Based on the public databases mentioned above,[57,60] the lysogeny ratios of phage contigs paired with dominant phyla were consistently higher than 60% accordingly (Figure S10B, p

https://doi.org/10.1021/acs.est.3c05452
Environ. Sci. Technol. 2023, 57, 17324−17337

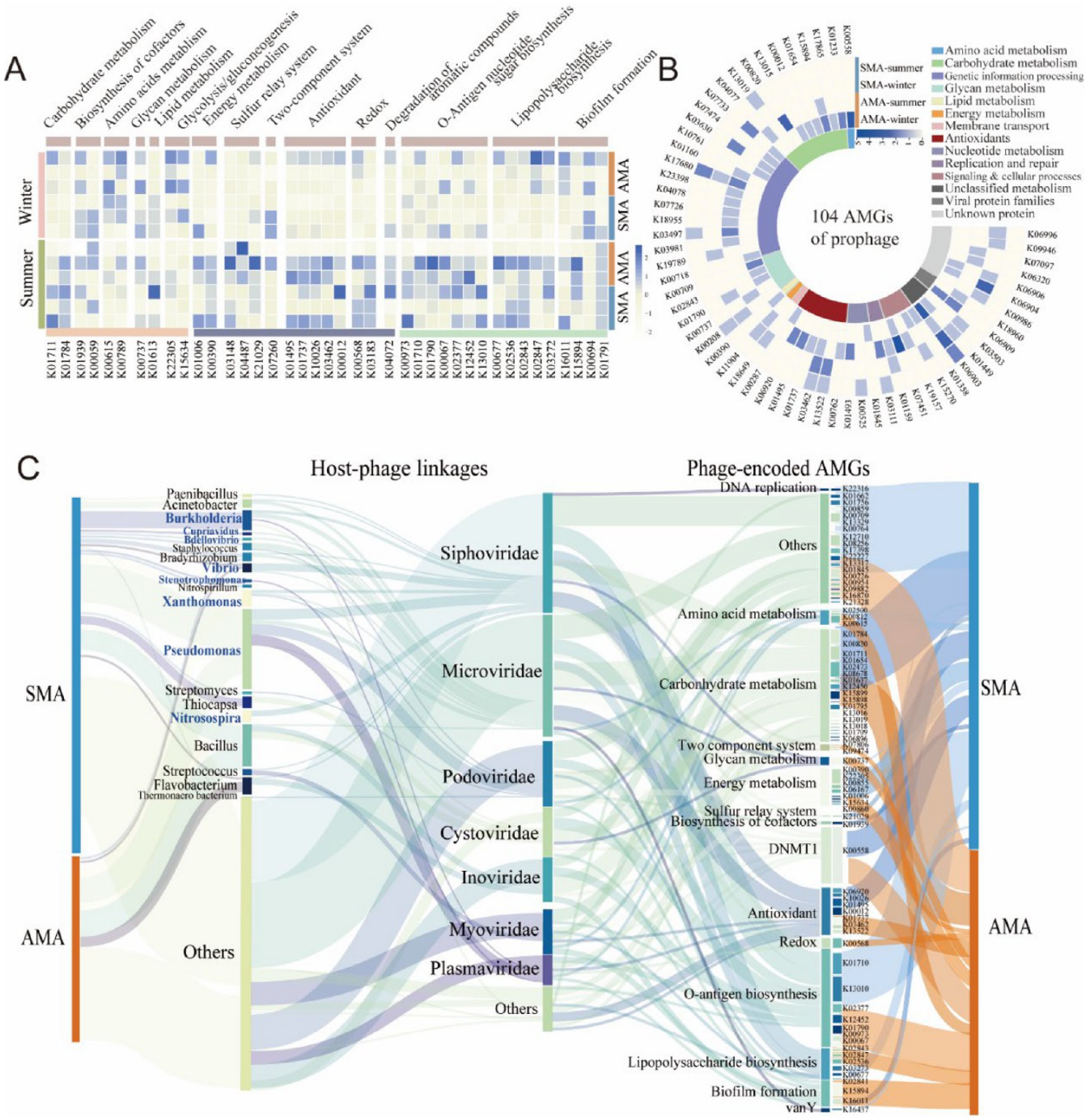

Figure 4. Distribution of phage-encoded AMGs detected in virome and phage−host linkages. (A) Distribution of typical viral-encoded AMGs in the KEGG functional pathway. AMGs were classified into three categories according to their potential function (i.e., fundamental metabolism (light orange), peripheral functions (dark gray), and aggregate stability (light green)). (B) The AMGs detected in potential prophage contigs were classified into 11 functional categories and 3 unclassified categories according to the occurrence numbers of AMGs. (C) Sankey plot presenting the distribution of AMGs in the phage−hosts linkage. More linkages were distributed in the SMA group. The species (in blue fonts) linkages and species with more linkages (in black fonts) of interest are displayed. The ratio (node width) of diverse AMGs annotated in the KEGG functional pathway was calculated based on the occurrence numbers. Different colors were used to distinguish between nodes, and the colors of edges were according to the nodes.

< 0.05). Compared to the distribution of prophage, the scaffolds carrying lysogenic markers showed a consistent pattern in the winter group with higher abundance in AMA. In contrast, more lysogenic markers were detected in SMA-summer, which was potentially associated with active phage−host interaction (Figure 3C and Figure S10C). At the genus level, the highest fraction of infected habitat generalists reached 49% of their total abundance (Figure 3E and S11A, $p < 0.05$). The high lysogenicity of phageome and bacteriome has also been reported in recent investigations of virome in a wastewater treatment plant.[87] Similar to other habitats under elevated environmental stress, phage community tended to exhibit a broad host range[20,43,44] when colonized to the

https://doi.org/10.1021/acs.est.3c05452
Environ. Sci. Technol. 2023, 57, 17324−17337

membrane surface facing great hydraulic pressure, along with other environmental stresses.

Bacterium−Phage Interactions Differed between Habitats and Seasons. The most phage−host linkages were observed in SMA-summer (279 linkages) followed by AMA-winter (201 linkages), SMA-winter (164 linkages), and AMA-summer (143 linkages) (Figure 3D). The highest fraction of putative prophages (2.25-fold, $p < 0.01$) and more vOTUs linked to more than one host (42% vs 34%, relative to SMA-winter; Figure S9A) were both observed in the AMA-winter virome. Moreover, the linkages between high-quality vOTUs and hosts were analyzed in parallel with the linkages between total vOTUs and hosts (Figure S9B). Among the 88 high-quality vOTUs−host linkages (50 vOTUs), 38% vOTUs were linked to more than one host, with 40% from AMA-winter vOTUs and 33% from SMA-summer vOTU, which is consistent with the trend in the whole 791 vOTUs−host linkages. Habitat specific species and biofilm core taxa in AMA were in a higher fraction (29% vs 23%, $p < 0.05$) relative to those in SMA (Figure 3E). The more bacterium−phage linkages and high abundance of biofilm core taxa (Figure S6D) found in AMA-winter suggested that the potential effect of phages on the structure of the microbial community may be more important in AMA than in SMA under the more hostile environment. Meanwhile, the host prediction results from the three in silico methods were coupled to represent putative phage−host associations based on their distinctive genomic characteristics, and these findings may require further verification due to the intrinsic limitations of bioinformatic analysis.[63]

Environmental stress could promote a symbiotic bacterium−phage relationship as phages in the lysogenic state may facilitate host adaptation to the hostile environment, thus benefiting its own survival.[88] The nonmotile phage would be impeded in the encounter and adsorption of host bacterium under the hydraulic environment.[89] The phage community remained in microbial aggregates with a 60% lysogenicity ratio that potentially survived the drastically changed hydraulic pressure in the MBR system (nearly 30 kPa hydraulic pressure on the membrane surface, while 0.5 kPa in the MBR tank). Lysogenic phages conceivably avoided progeny virion loss by conserving the phage genome within the host under complex environmental stress.

The active microbial metabolism in SMA in the summer could provide continuous host resources for phage propagation, while the high PS concentration (1.66−2.14-fold, relative to SMA-summer) and high PS/PN ratio in AMA-summer (1.69-fold, relative to SMA-summer) could impede phage infection due to the physical barrier role of EPS.[90] Specifically, EPS can impede phage infection and protect internal host bacteria by the exopolysaccharides (PS), which carry abundant hydrophilic and hydrophobic groups and exhibit great adsorption ability. The high concentration of the PS component, as well as the ratio of PS/PN in the AMA-summer aggregates (Figure S4B), apparently decreased phage mobility and thus impeded phage infection. In the AMA, the lower abundance of bacterial function genes in the KEGGL2 level (Figure 2B) suggested the suppressed cell metabolism, which was unfavorable for phage replication and assembly in host cells.[91] Consistently, the AMA group exhibited higher ratios of lysogeny in phage−host pairs (67% vs 53%) and prophage abundance (2.1% vs 0.57%) relative to SMA.

Temperature directly affected the bacterial community and bacterium−phage interactions. The composition of the bacterial and phage communities was significantly correlated with temperature varying by more than 10 °C between winter and summer (Figure S1D and Figure S12, Mantel's test, $p < 0.01$). In AMA, the decreased EPS concentration (0.54-fold, relative to AMA-summer) and abundant phage particle collection (reached 1.2×10^8 VLPs $g \cdot ss^{-1}$) in AMA-winter potentially contributed to the encounter of bacterium and phage.[92] However, there was a higher PS/PN ratio (1.37-fold) in SMA, and higher levels of genes were associated with cell lifecycle pathways in the winter groups (Figure 2B and Figure S5C). Moreover, the lysogeny ratio in SMA-winter was significantly lower than that in SMA-summer (53% vs 78%, t test, $p < 0.05$). Overall, the low temperature increased the environmental stress, especially in AMA, leading to more distinct bacterium−phage interactions between SMA and AMA. Seasonal changes greatly affect the lifecycle and metabolism of microbes, thus influencing microbial interactions and aggregation.[76] Our study suggested that seasonality is significantly associated with phage abundance and their interactions with hosts, which should be taken into consideration in future research.

Diverse Phage-Carried AMGs Contributed to Bacterial Survival in Different Habitats. AMGs are prevalently carried by phage genomes and play pivotal roles in modulating microbial metabolisms and element biogeochemical cycles.[18] A total of 238 types of pAMGs were annotated based on the KEGG database, with 52 types carried by both prophage and phage contigs (Figure 4A,B) and 75 types carried by high-quality vOTUs (Figure S13A). Interestingly, the relative abundance of pAMGs in extracellular phages showed no significant difference across habitats (Figure S13B). However, the relative abundance of AMGs carried by prophages in AMA was 2.91-fold higher than that in SMA (Figure S14A, $p < 0.01$). Furthermore, there were 17 types of pAMGs related to element metabolism (e.g., *ppdk* for carbon fixation, *cysH* for sulfur metabolism, and *phoN* for phosphate transport (Figure S13A)), which were mainly distributed in the SMA group (60.33%). The pAMGs related to broad substrate utilization (e.g., *adhE* and *adhP*, acetaldehyde/alcohol dehydrogenase) and biosynthesis of antioxidants (e.g., *UGDH*, *queE*, *NAMPT*, and *ubiG*) were widely distributed in the AMA group (54.06%) (Figure S14D,E). Consistently, 11.67% of prophage-carried AMGs in the AMA group were related to the biosynthesis of antioxidants (Figure 4B).

Phages could compensate for bacterial adaptability and exhibited specific patterns in habitat patterns facing different environmental stresses.[93] The pAMGs related to energy metabolism might enhance nutrient utilization and thus fitness advantages for bacterial hosts in SMA. The pAMGs related to the biosynthesis of antioxidants could confer tolerance of bacterial hosts to oxidative stress in AMA (e.g., membrane cleaning chemicals). In return, the improved fitness of bacterial hosts might facilitate phage survival and propagation. Specifically, 239 host-linked phage contigs encoded AMGs (65 belong to AMA), with 51 phage contigs linked to habitat generalists (18 belonging to AMA). There were 29.82 and 24.28% pAMGs associated with cell integrity and stress tolerance (e.g., lipopolysaccharide (LPS) biosynthesis) in the host linkages of AMA and SMA, respectively (Figure 4C). Therefore, the phages potentially contributed to the microbiome stability and function via AMGs.

https://doi.org/10.1021/acs.est.3c05452
Environ. Sci. Technol. 2023, 57, 17324−17337

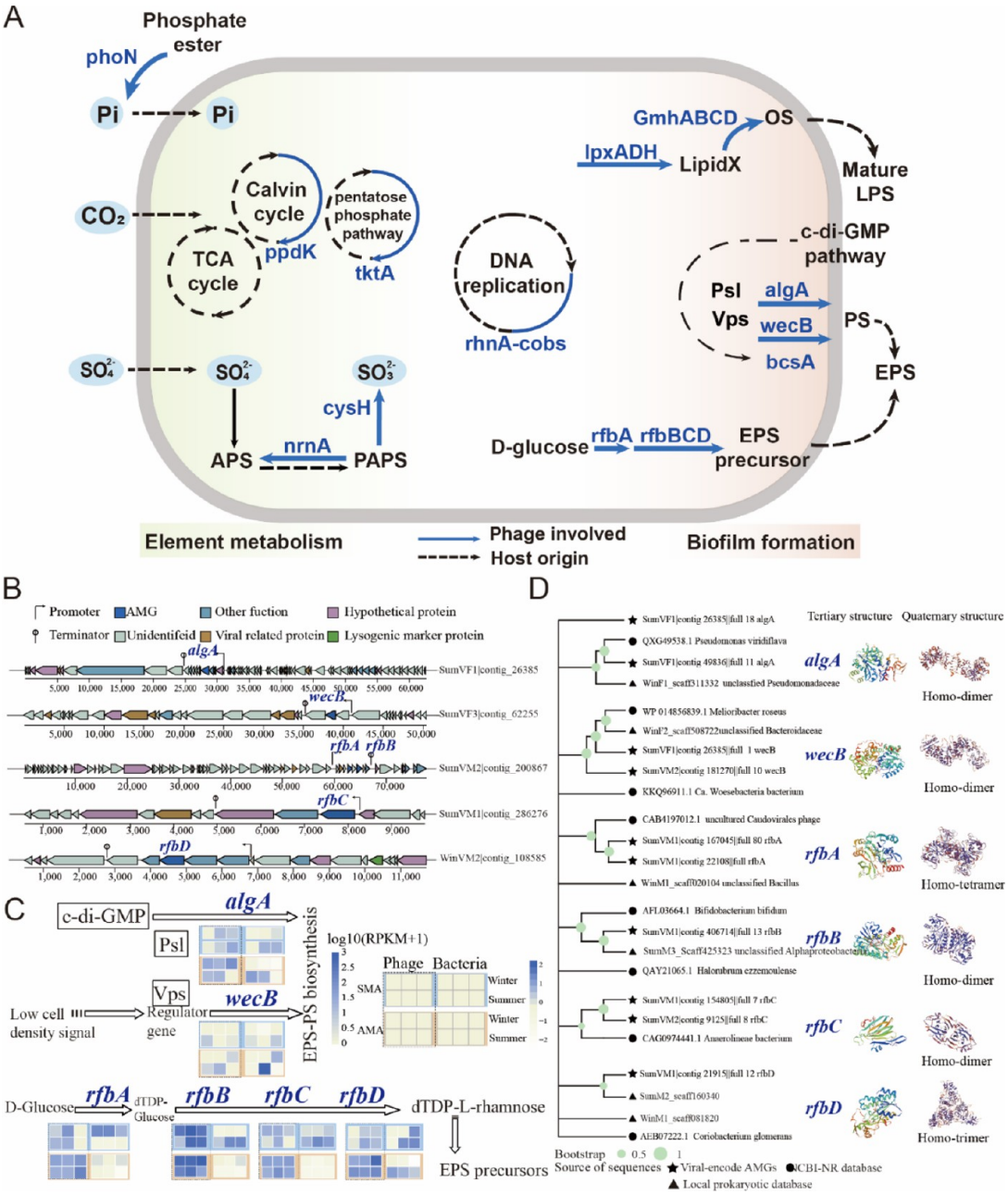

Figure 5. Genomic analyses of phage-encoded AMGs associated with EPS synthesis. (A) Conceptual depiction of metabolic functions of bacteria and pAMGs carried by high-quality vOTUs in pathways of element metabolism (light green) and biofilm formation (light pink). The pAMGs (in blue font) involved pathways were represented by blue arrows and the host origin ones by black dotted arrows. (B) Gene maps of five representative phage contigs harboring the AMGs of interest. The pAMGs (with names annotated in dark blue fonts), other function genes, hypothetical protein genes, and lysogenic marker genes are highlighted in dark blue, light blue, purple, brown, and green, respectively. (C) Relative abundance of the genes of interest in the virome (pAMGs) and in the bacteriome (functional genes). The phage-encoded *algA* and *wecB* genes' auxiliary metabolism in PS biosynthesis of EPS and the phage-encoded *rfbABCD* genes' auxiliary metabolism in L-rhamnolipid synthesis were discovered. (D) The maximum likelihood phylogenetic trees with cutoff >0.5 were constructed with reported AMGs (marked with asterisks), reference genes from the NCBI NR database (circles), and genes annotated in local prokaryotic sequences (triangles). The predicted protein structures of the reported AMGs were displayed accordingly.

AMGs associated with EPS synthesis are potentially involved in modulating host interactions and affecting the structure of aggregates (Figure 5). Generally, 32.03% of pAMGs were annotated for biofilm formation, including *bcsA* encoding cellulose synthase, *LpxADH* associated with LPS (Lipopolysaccharides) biosynthesis, *algA* associated with polysaccharides biosynthesis,[94] and *rfbABCD* associated with the EPS structure[95] (Figure 5A,B). Notably, consistent distribution patterns of genes related to PS synthesis were displayed in bacteria and pAMGs of the SMA group (Figure 5C). On the contrary, the genes in the L-rhamnose synthesis pathway displayed the opposite pattern by showing a high abundance in the phage-encoded AMGs but correspondingly lower in the bacteria-encoded genes, especially in AMA-winter groups. Consistently, the genes related to biofilm formation and EPS secretion encoded by bacteria were of high abundance in

https://doi.org/10.1021/acs.est.3c05452
Environ. Sci. Technol. 2023, 57, 17324−17337

winter, supporting the production of the EPS matrix under adverse environments (Figure S13C). The function of pAMG-encoded proteins was verified by the in silico methods, which further support their potential ecological functions for aggregation (Figure 5D and Figure S15). Compared to the in vitro expression, these methods are widely used for the high-throughput analysis of functional genes.[18] The distribution pattern of pAMGs indicated that the phages potentially served as reservoirs and vectors for functional genes related to structural stability.

■ ENVIRONMENTAL IMPLICATIONS

Our metagenomic and viromic study revealed that in MBR systems, the majority of phages were symbiotic with dominant species and habitat generalists, and the phage-carried diverse AMGs encoded genes associated with element metabolism and biofilm formation. These results suggested that symbiotic phages could have been involved in microbial metabolism and aggregate stability and thus were important for the microbial community in the hydraulic environment. Phages facing more hostile environmental stress on the membrane surface tended to form an enhanced symbiosis with bacterial communities by carrying AMGs associated with the functional and structural stability of microbial aggregates. Although the activity of pAMGs needed further experimental corroboration, our results from microscopy imaging and bioinformatic analyses strongly support the importance of environmental context on bacterium−phage interactions and the potential of the phage in determining microbiome structures and functions. From the application perspective, the microbial network analysis provides insights into bacterial and bacterium−phage interactions within the microbial aggregates, which generates hypotheses of microbial interactions in aggregate flocculation that are worth further testing.

■ ASSOCIATED CONTENT

Data Availability Statement

All bacterial and viral metagenomic raw reads generated in this study were submitted to NCBI under BioProject No. PRJNA943581.

Supporting Information

The Supporting Information is available free of charge at https://pubs.acs.org/doi/10.1021/acs.est.3c05452.

Details of the EEM spectra analysis of EPS, details of network analysis of microbial community, details of VBR calculation, and details of the structure prediction of pAMGs encoding protein as well as the water quality and quantity, water temperature and pH, transmembrane pressure during the sampling period, and pressure in the full-scale MBR, fluorescence microscopic images of phage particles, analysis of the EPS profile, microbial composition and functions annotation, analysis of phage communities profiles and clusters networks, lysogenicity of bacteriome and phageome, analysis of phage−host linkages predicted based on the public and local databases, analysis of the correlation between environmental factors and biotic factors, and analysis of distribution and types of phage- and prophage-carried AMGs (PDF)

List and identification of keystone species, habitat specific species, and habitat generalists identified in this study, list of core taxa of activated sludge and biofilm from reference, quality check of vOTUs, quality check and annotation of phage−host linkages, quality check and function annotation of phage- and prophage-carried AMGs, and list of lysogenic markers in pfam database (XLSX)

■ AUTHOR INFORMATION

Corresponding Authors

Pingfeng Yu − *College of Environmental and Resource Sciences, Zhejiang University, Hangzhou 310058, China; Innovation Center of Yangtze River Delta, Zhejiang University, Jiashan 314100, China;* orcid.org/0000-0003-0402-773X; Email: yupf@zju.edu.cn

Liang Zhu − *College of Environmental and Resource Sciences, Zhejiang University, Hangzhou 310058, China; Innovation Center of Yangtze River Delta, Zhejiang University, Jiashan 314100, China;* orcid.org/0000-0002-0921-7076; Email: felix79cn@zju.edu.cn

Authors

Yixiao Tan − *College of Environmental and Resource Sciences, Zhejiang University, Hangzhou 310058, China*

Dan Huang − *College of Environmental and Resource Sciences, Zhejiang University, Hangzhou 310058, China*

Mengting Maggie Yuan − *Department of Environmental Science, Policy, and Management, University of California, Berkeley, California 94720, United States*

Zhuodong Yu − *College of Environmental and Resource Sciences, Zhejiang University, Hangzhou 310058, China*

Huijie Lu − *College of Environmental and Resource Sciences, Zhejiang University, Hangzhou 310058, China;* orcid.org/0000-0002-0076-4508

Pedro J.J. Alvarez − *Civil and Environmental Engineering Department, Rice University, Houston, Texas 77005, United States;* orcid.org/0000-0002-6725-7199

Complete contact information is available at: https://pubs.acs.org/10.1021/acs.est.3c05452

Notes

The authors declare no competing financial interest.

■ ACKNOWLEDGMENTS

We thank Prof. Ye Mao and Dr. Ruonan Sun for their valuable advice on the data analysis and manuscript editing. This work was financially supported by National Natural Science Foundation of China (51961125101), Zhejiang Province Science and Technology Projects (2021C03021 and 2023C03131), National Natural Science Foundation of China (42277418), Key Program of the National Natural Science Foundation of China (52030003), the Fundamental Research Funds for the Central Universities (2023-KYY-514103-0005), and NSF ERC on Nanotechnology-Enabled Water Treatment (EEC-1449500).

■ REFERENCES

(1) Karygianni, L.; Ren, Z.; Koo, H.; Thurnheer, T. Biofilm Matrixome: Extracellular Components in Structured Microbial Communities. *Trends Microbiol.* **2020**, *28* (8), 668−681.

(2) Arnaouteli, S.; Bamford, N. C.; Stanley-Wall, N. R.; Kovács, Á. T. Bacillus Subtilis Biofilm Formation and Social Interactions. *Nat. Rev. Microbiol.* **2021**, *19* (9), 600−614.

(3) Flemming, H.-C.; Wuertz, S. Bacteria and Archaea on Earth and Their Abundance in Biofilms. *Nat. Rev. Microbiol.* **2019**, *17* (4), 247−260.
(4) de la Fuente-Núñez, C.; Reffuveille, F.; Fernández, L.; Hancock, R. E. Bacterial Biofilm Development as a Multicellular Adaptation: Antibiotic Resistance and New Therapeutic Strategies. *Curr. Opin. Microbiol.* **2013**, *16* (5), 580−589.
(5) Galand, P. E.; Pereira, O.; Hochart, C.; Auguet, J. C.; Debroas, D. A Strong Link between Marine Microbial Community Composition and Function Challenges the Idea of Functional Redundancy. *ISME J.* **2018**, *12* (10), 2470−2478.
(6) Ali, M.; Wang, Z.; Salam, K. W.; Hari, A. R.; Pronk, M.; van Loosdrecht, M. C. M.; Saikaly, P. E. Importance of Species Sorting and Immigration on the Bacterial Assembly of Different-Sized Aggregates in a Full-Scale Aerobic Granular Sludge Plant. *Environ. Sci. Technol.* **2019**, *53* (14), 8291−8301.
(7) Aqeel, H.; Basuvaraj, M.; Hall, M.; Neufeld, J. D.; Liss, S. N. Microbial Dynamics and Properties of Aerobic Granules Developed in a Laboratory-Scale Sequencing Batch Reactor with an Intermediate Filamentous Bulking Stage. *Appl. Microbiol. Biotechnol.* **2016**, *100* (1), 447−460.
(8) Sadiq, F. A.; Hansen, M. F.; Burmølle, M.; Heyndrickx, M.; Flint, S.; Lu, W.; Chen, W.; Zhang, H. Trans-Kingdom Interactions in Mixed Biofilm Communities. *FEMS Microbiol. Rev.* **2022**, *46* (5), fuac024.
(9) Niederdorfer, R.; Peter, H.; Battin, T. J. Attached Biofilms and Suspended Aggregates Are Distinct Microbial Lifestyles Emanating from Differing Hydraulics. *Nat. Microbiol.* **2016**, *1* (12), 1−7.
(10) Cai, W.; Cai, L.; Zhao, J.; Yao, H. Prokaryotic Community Interchange between Distinct Microhabitats Causes Community Pressure on Anammox Biofilm Development. *Water Res.* **2023**, *233*, No. 119726.
(11) Liu, W.; Jacquiod, S.; Brejnrod, A.; Russel, J.; Burmølle, M.; Sørensen, S. J. Deciphering Links between Bacterial Interactions and Spatial Organization in Multispecies Biofilms. *ISME J.* **2019**, *13* (12), 3054−3066.
(12) Chevallereau, A.; Pons, B. J.; van Houte, S.; Westra, E. R. Interactions between Bacterial and Phage Communities in Natural Environments. *Nat. Rev. Microbiol.* **2022**, *20* (1), 49−62.
(13) Zimmerman, A. E.; Howard-Varona, C.; Needham, D. M.; John, S. G.; Worden, A. Z.; Sullivan, M. B.; Waldbauer, J. R.; Coleman, M. L. Metabolic and Biogeochemical Consequences of Viral Infection in Aquatic Ecosystems. *Nat. Rev. Microbiol.* **2020**, *18* (1), 21−34.
(14) Pires, D. P.; Melo, L. D. R.; Azeredo, J. Understanding the Complex Phage-Host Interactions in Biofilm Communities. *Annu. Rev. Virol.* **2021**, *8* (1), 73−94.
(15) Shi, L.-D.; Dong, X.; Liu, Z.; Yang, Y.; Lin, J.-G.; Li, M.; Gu, J.-D.; Zhu, L.-Z.; Zhao, H.-P. A Mixed Blessing of Viruses in Wastewater Treatment Plants. *Water Res.* **2022**, *215*, No. 118237.
(16) Brown, M. R.; Baptista, J. C.; Lunn, M.; Swan, D. L.; Smith, S. J.; Davenport, R. J.; Allen, B. D.; Sloan, W. T.; Curtis, T. P. Coupled Virus - Bacteria Interactions and Ecosystem Function in an Engineered Microbial System. *Water Res.* **2019**, *152*, 264−273.
(17) Tang, X.; Fan, C.; Zeng, G.; Zhong, L.; Li, C.; Ren, X.; Song, B.; Liu, X. Phage-Host Interactions: The Neglected Part of Biological Wastewater Treatment. *Water Res.* **2022**, *226*, No. 119183.
(18) Yuan, L.; Ju, F. Potential Auxiliary Metabolic Capabilities and Activities Reveal Biochemical Impacts of Viruses in Municipal Wastewater Treatment Plants. *Environ. Sci. Technol.* **2023**, *57* (13), 5485−5498.
(19) Chen, Y.; Wang, Y.; Paez-Espino, D.; Polz, M. F.; Zhang, T. Prokaryotic Viruses Impact Functional Microorganisms in Nutrient Removal and Carbon Cycle in Wastewater Treatment Plants. *Nat. Commun.* **2021**, *12* (1), 5398.
(20) Liao, H.; Liu, C.; Ai, C.; Gao, T.; Yang, Q.-E.; Yu, Z.; Gao, S.; Zhou, S.; Friman, V.-P. Mesophilic and Thermophilic Viruses Are Associated with Nutrient Cycling during Hyperthermophilic Composting. *ISME J.* **2023**, *17*, 1−15.
(21) Padfield, D.; Castledine, M.; Buckling, A. Temperature-Dependent Changes to Host−Parasite Interactions Alter the Thermal Performance of a Bacterial Host. *ISME J.* **2020**, *14* (2), 389−398.
(22) Landsman, M. R.; Sujanani, R.; Brodfuehrer, S. H.; Cooper, C. M.; Darr, A. G.; Davis, R. J.; Kim, K.; Kum, S.; Nalley, L. K.; Nomaan, S. M.; Oden, C. P.; Paspureddi, A.; Reimund, K. K.; Rowles, L. S.; Yeo, S.; Lawler, D. F.; Freeman, B. D.; Katz, L. E. Water Treatment: Are Membranes the Panacea? *Annu. Rev. Chem. Biomol. Eng.* **2020**, *11* (1), 559−585.
(23) Matar, G. K.; Bagchi, S.; Zhang, K.; Oerther, D. B.; Saikaly, P. E. Membrane Biofilm Communities in Full-Scale Membrane Bioreactors Are Not Randomly Assembled and Consist of a Core Microbiome. *Water Res.* **2017**, *123*, 124−133.
(24) Jo, S. J.; Kwon, H.; Jeong, S.-Y.; Lee, C.-H.; Kim, T. G. Comparison of Microbial Communities of Activated Sludge and Membrane Biofilm in 10 Full-Scale Membrane Bioreactors. *Water Res.* **2016**, *101*, 214−225.
(25) Flemming, H.-C. Biofouling and Me: My Stockholm Syndrome with Biofilms. *Water Res.* **2020**, *173*, No. 115576.
(26) American Public Health Association; Rice, E. W.; Baird, R. B.; Eaton, A. D., eds., American Water Works Association, Water Environment Federation. *Standard Methods for the Examination of Water and Wastewater*, 22th ed.; APHA Press: Washington DC, 2012.
(27) Zhang, Z.; Ji, Y.; Cao, R.; Yu, Z.; Xu, X.; Zhu, L. A Novel Mode of Air Recycling Favored Stable Operation of the Aerobic Granular Sludge Process via Calcium Accumulation. *Chem. Eng. J.* **2019**, *371*, 600−608.
(28) Lowry, O.; Rosebrough, N.; Farr, A.; Randall, R. Protein Measurment with the Folin Phenol Reagent. *J. Biol. Chem.* **1951**, *193* (1), 265−275.
(29) Dubois, M.; Gilles, K.; Hamilton, J.; Rebers, P.; Smith, F. Colorimetric Method for Determination of Sugars and Related Substances. *Anal. Chem.* **1956**, *28* (3), 350−356.
(30) Bolger, A. M.; Lohse, M.; Usadel, B. Trimmomatic: A Flexible Trimmer for Illumina Sequence Data. *Bioinforma. Oxf. Engl.* **2014**, *30* (15), 2114−2120.
(31) Li, D.; Liu, C.-M.; Luo, R.; Sadakane, K.; Lam, T.-W. MEGAHIT: An Ultra-Fast Single-Node Solution for Large and Complex Metagenomics Assembly via Succinct de Bruijn Graph. *Bioinformatics* **2015**, *31* (10), 1674−1676.
(32) Fu, L.; Niu, B.; Zhu, Z.; Wu, S.; Li, W. CD-HIT: Accelerated for Clustering the next-Generation Sequencing Data. *Bioinformatics* **2012**, *28* (23), 3150−3152.
(33) Zhu, W.; Lomsadze, A.; Borodovsky, M. Ab Initio Gene Identification in Metagenomic Sequences. *Nucleic Acids Res.* **2010**, *38* (12), No. e132.
(34) Bushnell, B. *BBMap: A Fast, Accurate, Splice-Aware Aligner*. Lawrence Berkeley National Lab: Berkeley, CA 2014.
(35) Uritskiy, G. V.; DiRuggiero, J.; Taylor, J. MetaWRAP—a Flexible Pipeline for Genome-Resolved Metagenomic Data Analysis. *Microbiome* **2018**, *6* (1), 158.
(36) Chaumeil, P.-A.; Mussig, A. J.; Hugenholtz, P.; Parks, D. H. GTDB-Tk v2: Memory Friendly Classification with the Genome Taxonomy Database. *Bioinformatics* **2022**, *38* (23), 5315−5316.
(37) Nearing, J. T.; Douglas, G. M.; Hayes, M. G.; MacDonald, J.; Desai, D. K.; Allward, N.; Jones, C. M. A.; Wright, R. J.; Dhanani, A. S.; Comeau, A. M.; Langille, M. G. I. Microbiome Differential Abundance Methods Produce Different Results across 38 Datasets. *Nat. Commun.* **2022**, *13* (1), 342.
(38) Deng, Y.; Jiang, Y.-H.; Yang, Y.; He, Z.; Luo, F.; Zhou, J. Molecular Ecological Network Analyses. *BMC Bioinformatics* **2012**, *13* (1), 113.
(39) Xiao, N.; Zhou, A.; Kempher, M. L.; Zhou, B. Y.; Shi, Z. J.; Yuan, M.; Guo, X.; Wu, L.; Ning, D.; Van Nostrand, J.; Firestone, M. K.; Zhou, J. Disentangling Direct from Indirect Relationships in Association Networks. *Proc. Natl. Acad. Sci. U. S. A.* **2022**, *119* (2), No. e2109995119.
(40) Chen, Y.-J.; Leung, P. M.; Wood, J. L.; Bay, S. K.; Hugenholtz, P.; Kessler, A. J.; Shelley, G.; Waite, D. W.; Franks, A. E.; Cook, P. L.

M.; Greening, C. Metabolic Flexibility Allows Bacterial Habitat Generalists to Become Dominant in a Frequently Disturbed Ecosystem. *ISME J.* **2021**, *15*, 2986.
(41) Abdullah Al, M.; Xue, Y.; Xiao, P.; Xu, J.; Chen, H.; Mo, Y.; Shimeta, J.; Yang, J. Community Assembly of Microbial Habitat Generalists and Specialists in Urban Aquatic Ecosystems Explained More by Habitat Type than Pollution Gradient. *Water Res.* **2022**, *220*, No. 118693.
(42) von Meijenfeldt, F. A. B.; Hogeweg, P.; Dutilh, B. E. A Social Niche Breadth Score Reveals Niche Range Strategies of Generalists and Specialists. *Nat. Ecol. Evol.* **2023**, *7*, 1−14.
(43) Huang, D.; Yu, P.; Ye, M.; Schwarz, C.; Jiang, X.; Alvarez, P. J. J. Enhanced Mutualistic Symbiosis between Soil Phages and Bacteria with Elevated Chromium-Induced Environmental Stress. *Microbiome* **2021**, *9* (1), 150.
(44) Xia, R.; Sun, M.; Balcázar, J. L.; Yu, P.; Hu, F.; Alvarez, P. J. J. Benzo[a]Pyrene Stress Impacts Adaptive Strategies and Ecological Functions of Earthworm Intestinal Viromes. *ISME J.* **2023**, *17*, 1−11.
(45) Guo, J.; Bolduc, B.; Zayed, A. A.; Varsani, A.; Dominguez-Huerta, G.; Delmont, T. O.; Pratama, A. A.; Gazitúa, M. C.; Vik, D.; Sullivan, M. B.; Roux, S. VirSorter2: A Multi-Classifier, Expert-Guided Approach to Detect Diverse DNA and RNA Viruses. *Microbiome* **2021**, *9* (1), 37.
(46) Nayfach, S.; Camargo, A. P.; Schulz, F.; Eloe-Fadrosh, E.; Roux, S.; Kyrpides, N. C. CheckV Assesses the Quality and Completeness of Metagenome-Assembled Viral Genomes. *Nat. Biotechnol.* **2021**, *39* (5), 578−585.
(47) Ren, J.; Song, K.; Deng, C.; Ahlgren, N. A.; Fuhrman, J. A.; Li, Y.; Xie, X.; Poplin, R.; Sun, F. Identifying Viruses from Metagenomic Data Using Deep Learning. *Quant. Biol. Beijing China* **2020**, *8* (1), 64−77.
(48) Li, H.; Handsaker, B.; Wysoker, A.; Fennell, T.; Ruan, J.; Homer, N.; Marth, G.; Abecasis, G.; Durbin, R. 1000 Genome Project Data Processing Subgroup. The Sequence Alignment/Map Format and SAMtools. *Bioinforma. Oxf. Engl.* **2009**, *25* (16), 2078−2079.
(49) Bolduc, B.; Jang, H. B.; Doulcier, G.; You, Z.-Q.; Roux, S.; Sullivan, M. B. vConTACT: An iVirus Tool to Classify Double-Stranded DNA Viruses That Infect *Archaea* and *Bacteria*. *PeerJ.* **2017**, *5*, No. e3243.
(50) Wu, S.; Fang, Z.; Tan, J.; Li, M.; Wang, C.; Guo, Q.; Xu, C.; Jiang, X.; Zhu, H. DeePhage: Distinguishing Virulent and Temperate Phage-Derived Sequences in Metavirome Data with a Deep Learning Approach. *GigaScience* **2021**, *10* (9), giab056.
(51) Shang, J.; Tang, X.; Sun, Y. PhaTYP: Predicting the Lifestyle for Bacteriophages Using BERT. *Brief. Bioinform.* **2023**, *24* (1), bbac487.
(52) Mistry, J.; Chuguransky, S.; Williams, L.; Qureshi, M.; Salazar, G. A.; Sonnhammer, E. L. L.; Tosatto, S. C. E.; Paladin, L.; Raj, S.; Richardson, L. J.; Finn, R. D.; Bateman, A. Pfam: The Protein Families Database in 2021. *Nucleic Acids Res.* **2021**, *49* (D1), D412−D419.
(53) Roux, S.; Adriaenssens, E. M.; Dutilh, B. E.; Koonin, E. V.; Kropinski, A. M.; Krupovic, M.; Kuhn, J. H.; Lavigne, R.; Brister, J. R.; Varsani, A.; Amid, C.; Aziz, R. K.; Bordenstein, S. R.; Bork, P.; Breitbart, M.; Cochrane, G. R.; Daly, R. A.; Desnues, C.; Duhaime, M. B.; Emerson, J. B.; Enault, F.; Fuhrman, J. A.; Hingamp, P.; Hugenholtz, P.; Hurwitz, B. L.; Ivanova, N. N.; Labonté, J. M.; Lee, K.-B.; Malmstrom, R. R.; Martinez-Garcia, M.; Mizrachi, I. K.; Ogata, H.; Páez-Espino, D.; Petit, M.-A.; Putonti, C.; Rattei, T.; Reyes, A.; Rodriguez-Valera, F.; Rosario, K.; Schriml, L.; Schulz, F.; Steward, G. F.; Sullivan, M. B.; Sunagawa, S.; Suttle, C. A.; Temperton, B.; Tringe, S. G.; Thurber, R. V.; Webster, N. S.; Whiteson, K. L.; Wilhelm, S. W.; Wommack, K. E.; Woyke, T.; Wrighton, K. C.; Yilmaz, P.; Yoshida, T.; Young, M. J.; Yutin, N.; Allen, L. Z.; Kyrpides, N. C.; Eloe-Fadrosh, E. A. Minimum Information about an Uncultivated Virus Genome (MIUViG). *Nat. Biotechnol.* **2019**, *37* (1), 29−37.
(54) Shkoporov, A. N.; Hill, C. Bacteriophages of the Human Gut: The "Known Unknown" of the Microbiome. *Cell Host Microbe* **2019**, *25* (2), 195−209.
(55) Gregory, A. C.; Zablocki, O.; Howell, A.; Bolduc, B.; Sullivan, M. B. The Human Gut Virome Database. *bioRxiv* **2020**, *28*, 655910 DOI: 10.1101/655910.
(56) Gregory, A. C.; Zayed, A. A.; Conceição-Neto, N.; Temperton, B.; Bolduc, B.; Alberti, A.; Ardyna, M.; Arkhipova, K.; Carmichael, M.; Cruaud, C.; Dimier, C.; Domínguez-Huerta, G.; Ferland, J.; Kandels, S.; Liu, Y.; Marec, C.; Pesant, S.; Picheral, M.; Pisarev, S.; Poulain, J.; Tremblay, J. É.; Vik, D.; Babin, M.; Bowler, C.; Culley, A. I.; de Vargas, C.; Dutilh, B. E.; Iudicone, D.; Karp-Boss, L.; Roux, S.; Sunagawa, S.; Wincker, P.; Sullivan, M. B.; Acinas, S. G.; Babin, M.; Bork, P.; Boss, E.; Bowler, C.; Cochrane, G.; de Vargas, C.; Follows, M.; Gorsky, G.; Grimsley, N.; Guidi, L.; Hingamp, P.; Iudicone, D.; Jaillon, O.; Kandels-Lewis, S.; Karp-Boss, L.; Karsenti, E.; Not, F.; Ogata, H.; Pesant, S.; Poulton, N.; Raes, J.; Sardet, C.; Speich, S.; Stemmann, L.; Sullivan, M. B.; Sunagawa, S.; Wincker, P. Marine DNA Viral Macro- and Microdiversity from Pole to Pole. *Cell* **2019**, *177* (5), 1109−1123.
(57) Camargo, A. P.; Nayfach, S.; Chen, I.-M. A.; Palaniappan, K.; Ratner, A.; Chu, K.; Ritter, S. J.; Reddy, T. B. K.; Mukherjee, S.; Schulz, F.; Call, L.; Neches, R. Y.; Woyke, T.; Ivanova, N. N.; Eloe-Fadrosh, E. A.; Kyrpides, N. C.; Roux, S. IMG/VR v4: An Expanded Database of Uncultivated Virus Genomes within a Framework of Extensive Functional, Taxonomic, and Ecological Metadata. *Nucleic Acids Res.* **2023**, *51* (D1), D733−D743.
(58) Couvin, D.; Bernheim, A.; Toffano-Nioche, C.; Touchon, M.; Michalik, J.; Néron, B.; Rocha, E. P. C.; Vergnaud, G.; Gautheret, D.; Pourcel, C. CRISPRCasFinder, an Update of CRISRFinder, Includes a Portable Version, Enhanced Performance and Integrates Search for Cas Proteins. *Nucleic Acids Res.* **2018**, *46* (W1), W246−W251.
(59) Lowe, T. M.; Chan, P. P. tRNAscan-SE On-Line: Integrating Search and Context for Analysis of Transfer RNA Genes. *Nucleic Acids Res.* **2016**, *44* (W1), W54−W57.
(60) Shang, J.; Sun, Y. CHERRY: A Computational metHod for accuratE pRediction of Virus−pRokarYotic Interactions Using a Graph Encoder−Decoder Model. *Brief. Bioinform.* **2022**, *23*, bbac182.
(61) Shaffer, M.; Borton, M. A.; McGivern, B. B.; Zayed, A. A.; La Rosa, S. L.; Solden, L. M.; Liu, P.; Narrowe, A. B.; Rodríguez-Ramos, J.; Bolduc, B.; Gazitúa, M. C.; Daly, R. A.; Smith, G. J.; Vik, D. R.; Pope, P. B.; Sullivan, M. B.; Roux, S.; Wrighton, K. C. DRAM for Distilling Microbial Metabolism to Automate the Curation of Microbiome Function. *Nucleic Acids Res.* **2020**, *48* (16), 8883−8900.
(62) Kieft, K.; Zhou, Z.; Anantharaman, K. VIBRANT: Automated Recovery, Annotation and Curation of Microbial Viruses, and Evaluation of Viral Community Function from Genomic Sequences. *Microbiome* **2020**, *8* (1), 90.
(63) Pratama, A. A.; Bolduc, B.; Zayed, A. A.; Zhong, Z.-P.; Guo, J.; Vik, D. R.; Gazitúa, M. C.; Wainaina, J. M.; Roux, S.; Sullivan, M. B. Expanding Standards in Viromics: In Silico Evaluation of dsDNA Viral Genome Identification, Classification, and Auxiliary Metabolic Gene Curation. *PeerJ.* **2021**, *9*, No. e11447.
(64) Schwengers, O.; Jelonek, L.; Dieckmann, M. A.; Beyvers, S.; Blom, J.; Goesmann, A. Bakta: Rapid and Standardized Annotation of Bacterial Genomes via Alignment-Free Sequence Identification. *Microb. Genomics* **2021**, *7* (11), No. 000685.
(65) Tamura, K.; Stecher, G.; Kumar, S. MEGA11: Molecular Evolutionary Genetics Analysis Version 11. *Mol. Biol. Evol.* **2021**, *38* (7), 3022−3027.
(66) Kelley, L. A.; Mezulis, S.; Yates, C. M.; Wass, M. N.; Sternberg, M. J. E. The Phyre2 Web Portal for Protein Modeling, Prediction and Analysis. *Nat. Protoc.* **2015**, *10* (6), 845−858.
(67) Waterhouse, A.; Bertoni, M.; Bienert, S.; Studer, G.; Tauriello, G.; Gumienny, R.; Heer, F. T.; de Beer, T. A. P.; Rempfer, C.; Bordoli, L.; Lepore, R.; Schwede, T. SWISS-MODEL: Homology Modelling of Protein Structures and Complexes. *Nucleic Acids Res.* **2018**, *46* (W1), W296−W303.
(68) The UniProt Consortium. UniProt: The Universal Protein Knowledgebase in 2023. *Nucleic Acids Res.* **2023**, *51* (D1), D523−D531.

(69) Bittrich, S.; Bhikadiya, C.; Bi, C.; Chao, H.; Duarte, J. M.; Dutta, S.; Fayazi, M.; Henry, J.; Khokhriakov, I.; Lowe, R.; Piehl, D. W.; Segura, J.; Vallat, B.; Voigt, M.; Westbrook, J. D.; Burley, S. K.; Rose, Y. RCSB Protein Data Bank: Efficient Searching and Simultaneous Access to One Million Computed Structure Models Alongside the PDB Structures Enabled by Architectural Advances. *J. Mol. Biol.* **2023**, *435* (14), No. 167994.
(70) Ho, Q. N.; Fettweis, M.; Spencer, K. L.; Lee, B. J. Flocculation with Heterogeneous Composition in Water Environments: A Review. *Water Res.* **2022**, *213*, No. 118147.
(71) Yu, H.-Q. Molecular Insights into Extracellular Polymeric Substances in Activated Sludge. *Environ. Sci. Technol.* **2020**, *54* (13), 7742−7750.
(72) Artifon, V.; Zanardi-Lamardo, E.; Fillmann, G. Aquatic Organic Matter: Classification and Interaction with Organic Microcontaminants. *Sci. Total Environ.* **2019**, *649*, 1620−1635.
(73) Wu, L.; Ning, D.; Zhang, B.; Li, Y.; Zhang, P.; Shan, X.; Zhang, Q.; Brown, M. R.; Li, Z.; Van Nostrand, J. D.; Ling, F.; Xiao, N.; Zhang, Y.; Vierheilig, J.; Wells, G. F.; Yang, Y.; Deng, Y.; Tu, Q.; Wang, A.; Zhang, T.; He, Z.; Keller, J.; Nielsen, P. H.; Alvarez, P. J. J.; Criddle, C. S.; Wagner, M.; Tiedje, J. M.; He, Q.; Curtis, T. P.; Stahl, D. A.; Alvarez-Cohen, L.; Rittmann, B. E.; Wen, X.; Zhou, J. Global Diversity and Biogeography of Bacterial Communities in Wastewater Treatment Plants. *Nat. Microbiol.* **2019**, *4* (7), 1183−1195.
(74) Beier, S.; Andersson, A. F.; Galand, P. E.; Hochart, C.; Logue, J. B.; McMahon, K.; Bertilsson, S. The Environment Drives Microbial Trait Variability in Aquatic Habitats. *Mol. Ecol.* **2020**, *29* (23), 4605−4617.
(75) Banerjee, S.; Schlaeppi, K.; van der Heijden, M. G. A. Keystone Taxa as Drivers of Microbiome Structure and Functioning. *Nat. Rev. Microbiol.* **2018**, *16* (9), 567−576.
(76) Sun, C.; Zhang, B.; Ning, D.; Zhang, Y.; Dai, T.; Wu, L.; Li, T.; Liu, W.; Zhou, J.; Wen, X. Seasonal Dynamics of the Microbial Community in Two Full-Scale Wastewater Treatment Plants: Diversity, Composition, Phylogenetic Group Based Assembly and Co-Occurrence Pattern. *Water Res.* **2021**, *200*, No. 117295.
(77) Watanabe, T.; Miura, A.; Iwata, T.; Kojima, H.; Fukui, M. Dominance of *Sulfuritalea* Species in Nitrate-Depleted Water of a Stratified Freshwater Lake and Arsenate Respiration Ability within the Genus. *Environ. Microbiol. Rep.* **2017**, *9* (5), 522−527.
(78) Sharma, M.; Khurana, H.; Singh, D. N.; Negi, R. K. The Genus *Sphingopyxis*: Systematics, Ecology, and Bioremediation Potential - A Review. *J. Environ. Manage.* **2021**, *280*, No. 111744.
(79) Ma, Q.; Qu, Y.; Shen, W.; Zhang, Z.; Wang, J.; Liu, Z.; Li, D.; Li, H.; Zhou, J. Bacterial Community Compositions of Coking Wastewater Treatment Plants in Steel Industry Revealed by Illumina High-Throughput Sequencing. *Bioresour. Technol.* **2015**, *179*, 436−443.
(80) Ghosh, A.; Manna, M. C.; Jha, S.; Singh, A. K.; Misra, S.; Srivastava, R. C.; Srivastava, P. P.; Laik, R.; Bhattacharyya, R.; Prasad, S. S.; Singh, S. P.; Singh, S. K.; Kumar, V.; Tiwari, S.; Singh, A. K. Chapter Six - Impact of Soil-Water Contaminants on Tropical Agriculture, Animal and Societal Environment. In *Advances in Agronomy*; Sparks, D. L., Ed.; Academic Press, 2022; Vol. *176*, pp 209−274. DOI: 10.1016/bs.agron.2022.07.006.
(81) Kumar, A.; Trefault, N.; Olaniran, A. O. Microbial Degradation of 2,4-Dichlorophenoxyacetic Acid: Insight into the Enzymes and Catabolic Genes Involved, Their Regulation and Biotechnological Implications. *Crit. Rev. Microbiol.* **2016**, *42* (2), 194−208.
(82) Lin, Y.; Ye, G.; Luo, J.; Di, H. J.; Liu, D.; Fan, J.; Ding, W. *Nitrosospira* Cluster 8a Plays a Predominant Role in the Nitrification Process of a Subtropical Ultisol under Long-Term Inorganic and Organic Fertilization. *Appl. Environ. Microbiol.* **2018**, *84* (18), No. e01031.
(83) Yildiz, F. H.; Visick, K. L. Vibrio Biofilms: So Much the Same yet so Different. *Trends Microbiol.* **2009**, *17* (3), 109−118.
(84) Dutilh, B. E.; Cassman, N.; McNair, K.; Sanchez, S. E.; Silva, G. G. Z.; Boling, L.; Barr, J. J.; Speth, D. R.; Seguritan, V.; Aziz, R. K.; Felts, B.; Dinsdale, E. A.; Mokili, J. L.; Edwards, R. A. A Highly Abundant Bacteriophage Discovered in the Unknown Sequences of Human Faecal Metagenomes. *Nat. Commun.* **2014**, *5* (1), 4498.
(85) Jian, H.; Yi, Y.; Wang, J.; Hao, Y.; Zhang, M.; Wang, S.; Meng, C.; Zhang, Y.; Jing, H.; Wang, Y.; Xiao, X. Diversity and Distribution of Viruses Inhabiting the Deepest Ocean on Earth. *ISME J.* **2021**, *15*, 1−17.
(86) Runa, V.; Wenk, J.; Bengtsson, S.; Jones, B. V.; Lanham, A. B. Bacteriophages in Biological Wastewater Treatment Systems: Occurrence, Characterization, and Function. *Front. Microbiol.* **2021**, *12*, No. 730071, DOI: 10.3389/fmicb.2021.730071.
(87) Liu, R.; Li, Z.; Han, G.; Cun, S.; Hou, D.; Yu, Z.; Xue, K.; Liu, X. Microbial Density-Dependent Viral Dynamics and Low Activity of Temperate Phages in the Activated Sludge Process. *Water Res.* **2023**, *232*, No. 119709.
(88) Warwick-Dugdale, J.; Buchholz, H. H.; Allen, M. J.; Temperton, B. Host-Hijacking and Planktonic Piracy: How Phages Command the Microbial High Seas. *Virol. J.* **2019**, *16* (1), 15.
(89) Yu, Z.; Schwarz, C.; Zhu, L.; Chen, L.; Shen, Y.; Yu, P. Hitchhiking Behavior in Bacteriophages Facilitates Phage Infection and Enhances Carrier Bacteria Colonization. *Environ. Sci. Technol.* **2021**, *55* (4), 2462−2472.
(90) Zhang, B.; Yu, P.; Wang, Z.; Alvarez, P. J. J. Hormetic Promotion of Biofilm Growth by Polyvalent Bacteriophages at Low Concentrations. *Environ. Sci. Technol.* **2020**, *54* (19), 12358−12365.
(91) Fernández, L.; Rodríguez, A.; García, P. Phage or Foe: An Insight into the Impact of Viral Predation on Microbial Communities. *ISME J.* **2018**, *12* (5), 1171−1179.
(92) Hwang, Y.; Roux, S.; Coclet, C.; Krause, S. J. E.; Girguis, P. R. Viruses Interact with Hosts That Span Distantly Related Microbial Domains in Dense Hydrothermal Mats. *Nat. Microbiol.* **2023**, *8* (5), 946−957.
(93) Luo, X.-Q.; Wang, P.; Li, J.-L.; Ahmad, M.; Duan, L.; Yin, L.-Z.; Deng, Q.-Q.; Fang, B.-Z.; Li, S.-H.; Li, W.-J. Viral Community-Wide Auxiliary Metabolic Genes Differ by Lifestyles, Habitats, and Hosts. *Microbiome* **2022**, *10* (1), 190.
(94) Stoner, S. N.; Baty, J. J.; Scoffield, J. A. Pseudomonas Aeruginosa Polysaccharide Psl Supports Airway Microbial Community Development. *ISME J.* **2022**, *16* (7), 1730−1739.
(95) Wang, W.; Yan, Y.; Zhao, Y.; Shi, Q.; Wang, Y. Characterization of Stratified EPS and Their Role in the Initial Adhesion of Anammox Consortia. *Water Res.* **2020**, *169*, No. 115223.